LASER INTERFEROMETER GRAVITATIONAL WAVE OBSERVATORY
- LIGO -
CALIFORNIA INSTITUTE OF TECHNOLOGY
MASSACHUSETTS INSTITUTE OF TECHNOLOGY

Technical Note	**LIGO-T1600285-v1**	2016/09/23

Temperature control of silicon mirrors in locked cavities at 123 K *Final report*

Nizar Ezroura (Mentors: Chris Wipf and Johannes Eichholz)

Distribution of this document:
LIGO Scientific Collaboration

California Institute of Technology
LIGO Project, MS 18-34
Pasadena, CA 91125
Phone (626) 395-2129
Fax (626) 304-9834
E-mail: info@ligo.caltech.edu

Massachusetts Institute of Technology
LIGO Project, Room NW17-161
Cambridge, MA 02139
Phone (617) 253-4824
Fax (617) 253-7014
E-mail: info@ligo.mit.edu

LIGO Hanford Observatory
Route 10, Mile Marker 2
Richland, WA 99352
Phone (509) 372-8106
Fax (509) 372-8137
E-mail: info@ligo.caltech.edu

LIGO Livingston Observatory
19100 LIGO Lane
Livingston, LA 70754
Phone (225) 686-3100
Fax (225) 686-7189
E-mail: info@ligo.caltech.edu

http://www.ligo.caltech.edu/

Abstract

Thermal noise is one of the multiple areas in the LIGO noise budget that affects its overall sensitivity. One feature of a cryogenic LIGO is to reduce this noise by working at low temperatures. Investigations into this method at this stage were performed using short optical cavities made of silicon held at 123 K inside a cryostat. A 1550 nm laser beam has been locked into resonance to these cavities, using the PDH technique for frequency stabilization. At this temperature, the thermal expansion coefficient is at a zero-crossing point, and thus slight temperature fluctuations around that point stop translating into length fluctuations. A temperature control system has been designed, to monitor the mirror temperatures of the optical cavities setup and thus quantify deviations from resonance.

1 Introduction

LIGO (**L**aser **I**nterferometer **G**ravitational-wave **O**bservatory) is a large-scale observatory that was designed to detect gravitational waves, a prediction going back to Albert Einstein's 1916 theory of general relativity. As the name indicates, it is based on the principle of laser interferometry: it is a Michelson interferometer. The effect of gravitational waves from currently known astrophysical sources (such as binary black hole mergers) is very small, manifesting itself as a minute strain in the laser beam length, with expected peak values in the range of 10^{-21} (Fig. 1.1). With its four-kilometer-long arms (Fig. 1.2), the interferometer undergoes a peak length change of $4 \cdot 10^3 \cdot 10^{-21} = 4 \cdot 10^{-18}$ m

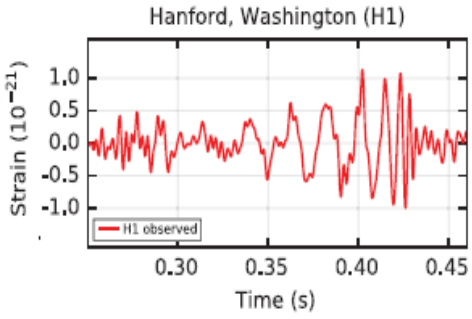

Figure 1.1 : The gravitational-wave event GW150914 observed by the LIGO Hanford. Times are shown relative to September 14, 2015 at 09:50:45 UTC [1]

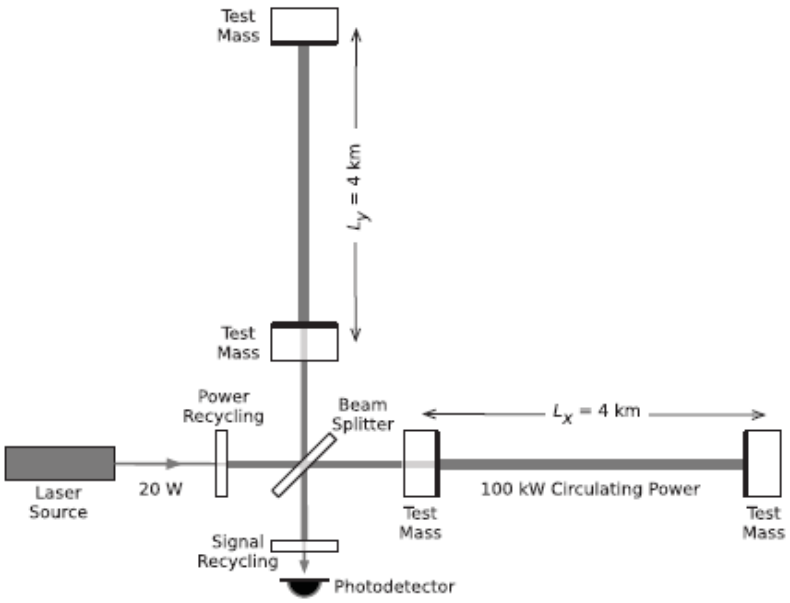

Figure 1.2 : A simplified layout of LIGO. [1]

As part of this enhanced interferometer, test masses are used to store laser power (acting as effective Fabry-Perot cavities). Each of these four test masses is a 40-kg cylinder made of fused silica. This material is chosen in consistency with the IR laser (low absorption at the operational $\lambda = 1064$nm) along with specific mirror coatings, amongst other mechanical and optical constraints (transmittance/reflectance, elastic and structural coefficients) [2].

Setting up these high-precision components, just like with other parts of LIGO, is justified by the extreme sensitivities involved in the experiment. The latter are quantitatively estimated by a plot of all noise sources as a function of frequency (Fig. 1.3). The different curves in the plot all refer to different areas that generate distinct noises. The prominent noise areas associated with the previously mentioned test masses are quantum shot noise (purple curve) and mirror coating Brownian noise terms (red curve). As with other noise sources in general, engineering ways to reduce these terms (i.e. lower the curves in this plot) brings the strain spectral density (the quantity in $1/\sqrt{\text{Hz}}$)down, and consequently allows for a higher sensitivity to low strain values in a given bandwidth.

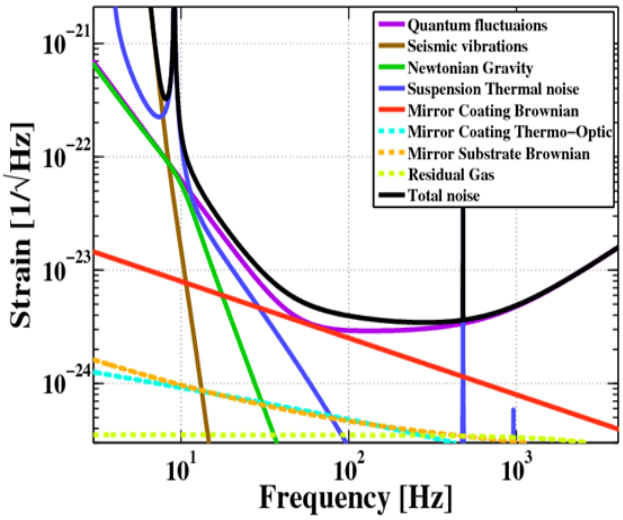

Figure 1.3: The noise budget in LIGO

The first term is related to quantum fluctuations. On a first level, it can be understood from the quantization of incoming light into photons, whose arrival on test masses is described a Poisson time process. This takes the form of quantum shot noise. More fundamentally though, it is related to quantum vacuum fluctuations entering the readout port of the interferometer. These are described by the Heisenberg uncertainty principle, between the amplitude and phase variables. Thus even in vacuum can there be fluctuations in the amplitude and phase of electromagnetic fields. Current LIGO technology such as quantum squeezing allows the reduction of one term (such as amplitude), and by virtue of the Heisenberg inequality "squeezing" that term and increasing the other. This yields then phase noise, which is mitigated by an inverse dependency on the input laser power P_{in} This can be justified by appealing to the phasor picture of the carrier beam: as a phasor $A \propto A_0(t)e^{i\varphi(t)}$, a longer vector with a given small $d\varphi$ gives a small relative fluctuations term $\frac{dA}{A}$

The second term, Brownian mirror coating noise, manifests as Brownian fluctuations in the coating material. These can be related with the help of the Fluctuation-Dissipation Theorem to temperature T and a dissipation contribution $R(\phi)$:

$$S_x(f) = 2k_B T R(\phi)$$

S_x represents the position noise in frequency space and $R(\phi)$ is a function of ϕ (the loss angle, a dimensionless quantity expressing the lossiness of the material), and of some mechanical constants of the material (Y the Young modulus and σ the Poisson ratio) and spatial characteristics of the incoming beam (w the half-width of a Gaussian beam for example) [4].

Reducing the first term would then appear to be facilitated with higher input laser power P_{in}. But increasing the latter indiscriminately causes problems on its own: namely thermal distortions in the test masses material. These can take the form of thermal lensing and spatial alterations in the distribution of the index of refraction along the material. A more judicious approach would be to work on reducing the thermal noise term. Given a choice of

material (currently fused silica) at a selected temperature, one is left with mechanical and optical properties of that environment. This indeed is the justification behind the proposed enhancement to the current Advanced LIGO: Cryogenic LIGO (also called LIGO Voyager). The trade-off of implementing mirror coatings and material at a cryogenic temperature would be an appreciable scaling-down of the thermal noise term.

The main candidate for a cryogenic LIGO design is crystalline silicon, at the particular operational temperature of 123 K. This value is in fact a temperature at which the coefficient of thermal expansion (CTE) goes to zero. The CTE actually changes sign in the vicinity of that zero-crossing point (Fig. 1.4); this alludes to the possibility of establishing a control system in that region. With limited thermo-elastic behavior at this point, increasing P_{in} can then yield reduced deformation of the mirror material. Cryogenic silicon also performs better mechanically compared to fused silica at the usual 300 K, as the latter's mechanical loss peaks as one goes to lower and lower temperatures [5] [6] [7]. To achieve these better properties with cryogenic silicon, it becomes necessary to work with a higher wavelength than the standard 1064 nm. $\lambda = 1550$ nm is the main alternative, as silicon is less absorptive at higher wavelengths; that specific wavelength is also a standard telecommunications wavelength, covered extensively by technical knowledge bases.

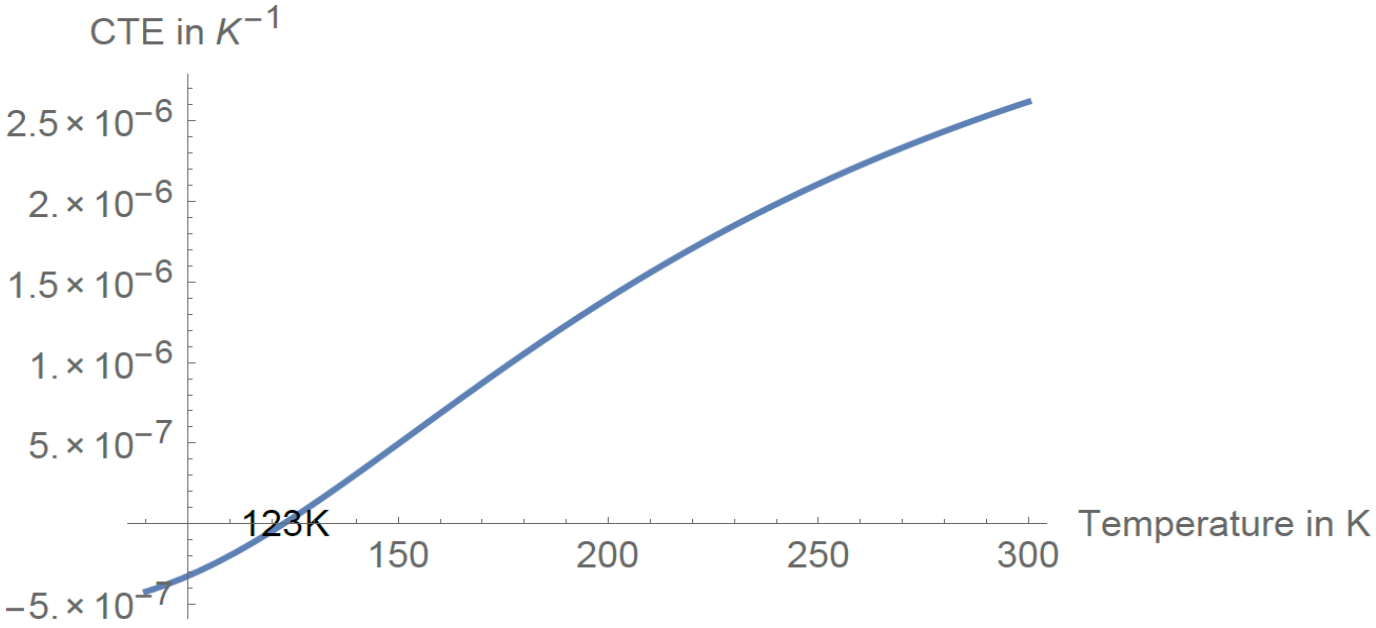

Figure 1.4: Plot of CTE vs. temperature. There are in fact two zero-crossing points to the CTE: the other one is at 18K. [8]

2 Experimental setup

In order to better investigate the noise behavior of desired mirror coatings and material (in this project's case, crystalline silicon), it proves useful to work on a specific experimental setup: a frequency-stabilized laser locked to a small Fabry-Perot cavity [9]. Once the system is tested at room temperature, it can be further tested at 123 K to verify the merits of cryogenic silicon concerning thermal noise limitation.

The main components that are configured to attain such a setup are the **Gaussian 1550 nm laser beam** and the **optical cavity** to which the laser will be **locked**.

2.1 Gaussian Beams

The standard lasers used for this type of experiments are Gaussian beams, named so as their intensity profile at a given cross-section follows a Gaussian spread:

$$I(x, y, z) \propto e^{-\frac{2(x^2+y^2)}{w(z)^2}}$$

where x and y are taken in the cross-section plane, z designates the beam path length at which the cross-section is taken, and $w(z)$ is the characteristic beam width at the specified z.

Propagating a solution to the wave equation $\nabla^2\psi + k^2\psi^2 = 0$ [10], one finds that the beam has two important variables: the characteristic width $w(z)$ and the radius of curvature of the wavefront $R(z)$. Both of these vary across the beam path in a particular way:

$$w(z) = w_0\sqrt{1 + \left(\frac{\lambda z}{\pi w_0^2}\right)^2} \quad \text{and} \quad R(z) = z\left(1 + \left(\frac{\pi w_0^2}{\lambda z}\right)^2\right)$$

The expression $w(z)$ describes a hyperbola that converges, then is minimal at $z = 0$ with $w(0) := w_0$, the **waist** of the laser beam. This helps define a characteristic path length, the Rayleigh range z_R defined as $w(z_R) = \sqrt{2}w_0$ and hence the range after which the cross-section doubles in area.

The expression $R(z)$ describes an odd function for the **radius of curvature** which is infinite at the waist location ($z = 0 \leftrightarrow w = w_0$); an infinite ROC being equivalent to a flat wavefront. It decreases gradually until it reaches a minimum at $z = z_R$ (strongest wavefront curvature at that range), and then increases again towards infinity as $z \to \infty$

For a Gaussian beam, the main experimental parameters are the waist w_0 and the waist location z_0. In fact, these parameters are only characteristics of the fundamental mode of the laser beam, as there is an entire family of solutions to the propagation equation. These

are called Hermite-Gaussian modes, or higher order modes, denoted T_{mn} (Fig. 2.1.1) where m and n are mode indices. A simple Gaussian profile (the T_{00} mode) is in general a good approximation for most laser beams, so the bulk of describing laser operation afterwards reduces to the fundamental parameters of the simple T_{00} mode.

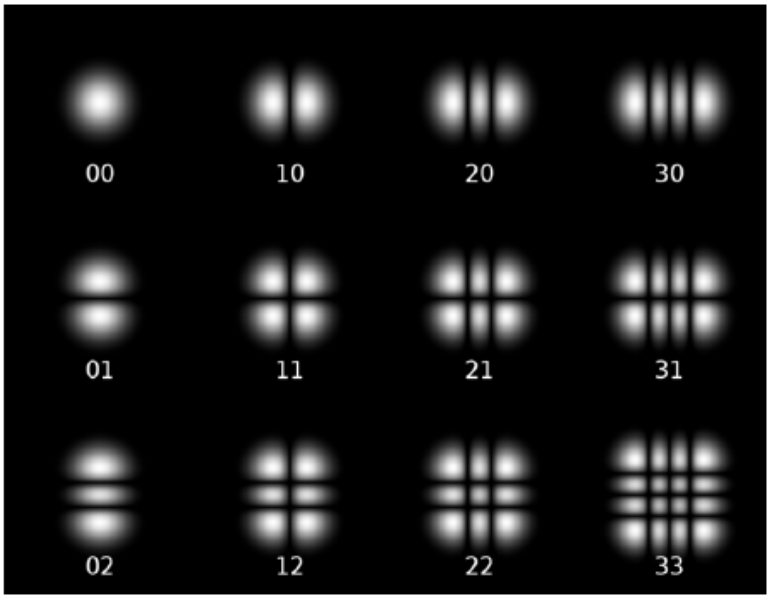

Figure 2.1.1: Twelve Hermite-Gaussian low-order modes ($m, n \leq 3$)

Obtaining the fundamental mode parameters is a necessary step towards setting up an optical setup for the cavity-locking. A knife-edge and a photodetector were used to perform the fundamental mode measurements, through the following protocol:

• Place the platform at a distance z away from the laser collimator;

• Obstruct the laser beam cross-section by progressively moving the knife-edge in. Record the transmitted voltage $V(d)$ on the photodetector as a function of the knife distance d.

• As the photovoltage is proportional to the incident power:

$$V(d) \propto \text{Power} \propto \int_{y=-\infty}^{+\infty} \int_{x=d}^{+\infty} e^{-\frac{2(x^2+y^2)}{w(z)^2}} dxdy \propto \left(1 - \text{erf}\left(\sqrt{2}\frac{d}{w(z)}\right)\right)$$

taking the form of a decreasing sigmoid characterized by a slope parameter $\frac{\sqrt{2}}{w(z)}$. Each set of $(d, V(d))$, after being fit to such a sigmoid (of general fit form $c_0 + c_1 \text{ erf}\Big(c_2(d - c_3)\Big)$), then yields the $w(z)$ corresponding to that distance z away from the laser collimator.

• The $(z, w(z))$ data points are then fit into $w(z) = w_0\sqrt{1 + \left(\frac{\lambda(z-z_0)}{\pi w_0^2}\right)^2}$

The experimental parameters obtained with this method are represented in this plot:

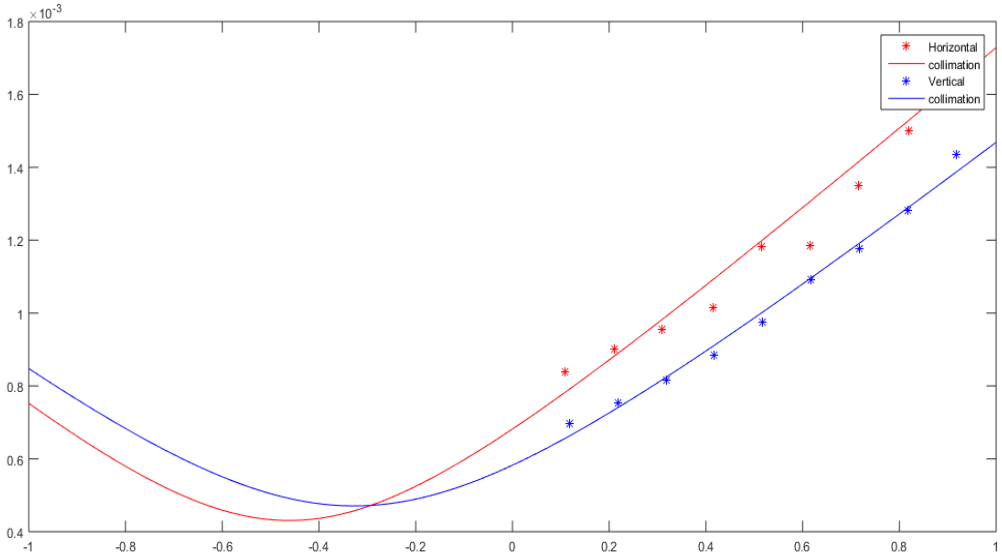

Fig. 2.1.2: Plot of beam width ($w(z)$ in m) vs. laser beam path (z in m), for the two different laser collimation orientations (slight astigmatism)

The two collimations yielded close waist values: $w_{0,x} = 430\mu$m and $w_{0,y} = 470\mu$m, at waist locations $w_{0,x} = -0.46$m and $w_{0,y} = -0.33$m.

2.2 Optical cavities

The obtained fundamental mode parameters are essential to the next step: arranging the optical system in order to obtain laser resonance in an optical cavity. This step is called **mode-matching**, as it involves fitting a fundamental mode (and possibly the other higher-order modes) to the specifications of an optical cavity.

An optical cavity can be described as two mirrors of pre-specified radii of curvature, spaced apart by L. This arrangement determines a resonance condition, such that:

$$\omega_N = N \cdot \frac{c}{2L}$$

This can be understood as fitting N (integer) multiples of an incident beam's wavelength $\lambda = \frac{c}{\omega}$ into the round-trip length $2L$. In frequency space, the spacing $\frac{c}{2L}$ is known as the **free spectral range** (**FSR**).

Another constraint that the cavity introduces concerns the wavefront of the incoming laser: the input mode of the laser has to match the cavity mode. The cavities used in the project were made of two mirrors with one-meter radii of curvature and $L = 4$". With these symmetric cavities, the waist (and hence the flat wavefront) is exactly $L/2$ away from the mirrors

(in the middle of the cavity). Then:

$$R(L/2) = 1 \text{ m} \rightarrow R(L/2) = (L/2)\left(1 + \left(\frac{\pi w_0^2}{\lambda L/2}\right)^2\right) = 1 \text{ m}$$

$$\rightarrow (4\text{”}/2)\left(1 + \left(\frac{\pi w_0^2}{(1550 \text{ nm})\, 4\text{”}/2}\right)^2\right) = 1 \text{ m}$$

$$\rightarrow w_0 = 329\ \mu\text{m} \text{ is the target waist for the cavity}$$

Given this target waist, the initial characteristic initial waist, and a total beam path length estimate, it becomes necessary to setup a series of lenses to bring the beam width to the right side (without lenses, the beam would just diverge as per $w(z)$). This happens as a lens of focal length f transforms an incoming beam with waist w located s behind the lens, into a beam with waist w' located t in front of the lens (Fig. 2.2.1) according to [11]:

$$w' = \frac{fw}{\sqrt{(f-s)^2 + \frac{\pi^2 w^4}{\lambda^2}}}$$

$$\frac{1}{t + \frac{\pi^2 (w')^4}{\lambda^2 (t-f)}} = \frac{1}{f} - \frac{1}{s}$$

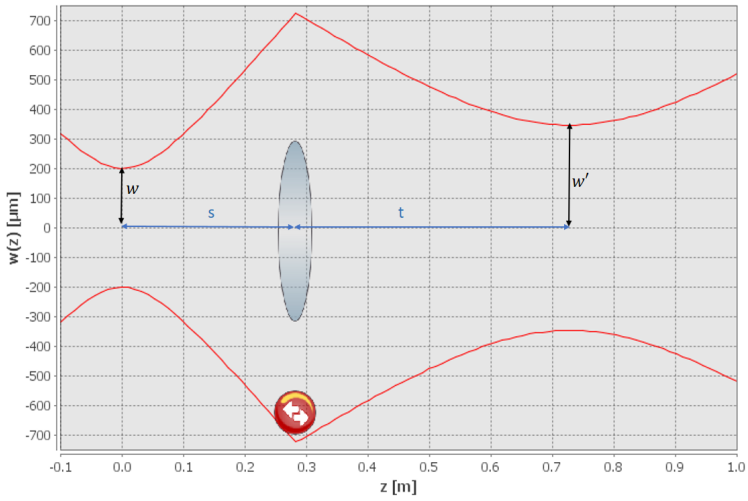

Fig. 2.2.1: Example of a lens computation on JAMMT applet, using $w = 200\ \mu$m and $s = 0.282$ m. The result is $t = 0.447$ m and $w' = 346\ \mu$m

The experimental setup for the project only required three lenses; a possible solution (possible lens positions and focal lengths) shown below (Fig. 2.2.2):

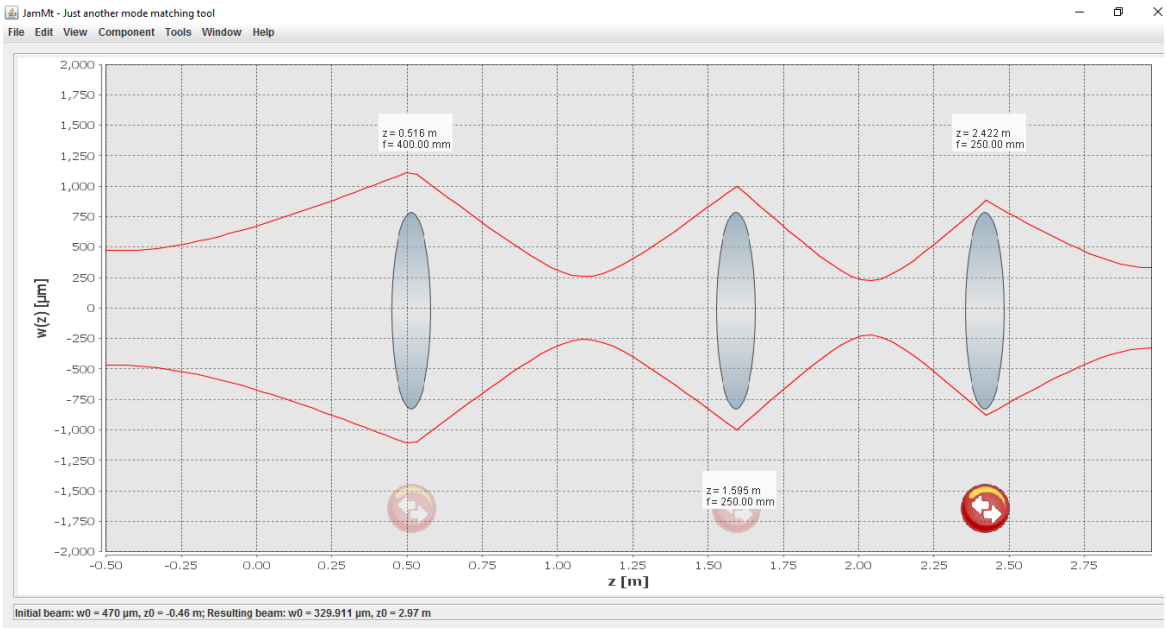

Fig. 2.2.2: Approximate three-lens solution given an initial 470 μm and target 330 μm waists.

After setting up and aligning the lenses to the target cavity, cavity resonances become accessible to observe (after setting up a CCD camera in transmission behind the cavity). To scan through frequency space to perceive the multiple T_{mn}, the laser temperature is dithered through by tuning the current driver. As there is no frequency stabilization at this point of the setup, the T_{00} can be seen but flickers as it is not yet stabilized.

2.3 Pound-Drever-Hall (PDH) frequency stabilization

In order to prepare stable cavities for temperature-related measurements, it is necessary to first implement a laser frequency stabilization technique. Such a technique would require receiving a variable error signal, in signed proportion to the deviation from resonance. The Pound-Drever-Hall technique satisfies these conditions, and is thus commonly used for locking lasers to cavities (i.e. stabilizing their frequencies via resonance). The basic method behind the PDH technique relies on generating sidebands by phase modulation in the beam going towards the cavity using a modulation frequency Ω. As these are frequency sidebands $\omega \pm \Omega$ (away from resonance at the laser frequency), they get reflected along with part of the carrier beam. This reflected signal is where the error signal mentioned above comes from.

Starting with an incident beam $e^{i\omega t}$, it becomes phase-modulated with depth β and modu-

lation frequency Ω:

$$e^{i(\omega t+\beta \sin \Omega t)} = e^{i\omega t} \sum_{n=-\infty}^{+\infty} J_n(\beta) e^{in\Omega} \text{ (using Jacobi-Anger expansion)}$$

$$e^{i(\omega t+\beta \sin \Omega t)} = e^{i\omega t} \left(J_0(\beta) + \sum_{n=0}^{+\infty} J_{2n+1}(\beta)(e^{i(2n+1)\Omega} - e^{-i(2n+1)\Omega}) + \sum_{n=1}^{+\infty} J_{2n}(\beta)(e^{i(2n)\Omega} + e^{-i(2n)\Omega}) \right)$$

using the fact that $J_{-n}(\beta) = (-1)^n J_n(\beta)$ for nth-order Bessel functions of the first kind J_n. For a frequency component $m\Omega$, the associated field amplitude is proportional to $J_m(\beta)$ and thus the power becomes proportional to $J_m(\beta)^2$.

For usual modulation depths satisfying $\beta < 1$, orders higher than ± 1 can be discarded (the power in high-order sidebands is practically small), and thus:

$$e^{i(\omega t+\beta \sin \Omega t)} \approx e^{i\omega t} \left(J_0(\beta) + J_1(\beta) e^{i\Omega t} - J_1(\beta) e^{-i\Omega t} \right)$$

$$= J_0(\beta) e^{i\omega t} + J_1(\beta) e^{i(\omega+\Omega)t} - J_1(\beta) e^{i(\omega-\Omega)t}$$

The spectrum then mainly consists of a peak carrier frequency peak with power $\propto J_0(\beta)^2$ at ω, and two sidebands with power $\propto J_1(\beta)^2$ at $\omega \pm \Omega$. Given a cavity with a complex reflection coefficient $F(\omega) = \frac{E_{ref}(\omega)}{E_{inc}(\omega)}$, this takes the slightly different form:

$$E_{ref} = E_0 J_0(\beta) e^{i\omega t} F(\omega) + E_0 J_1(\beta) e^{i(\omega+\Omega)t} F(\omega+\Omega) - E_0 J_1(\beta) e^{i(\omega-\Omega)t} F(\omega-\Omega)$$

given $E_{inc} = E_0 e^{i\omega t}$

Powers, not complex field amplitudes, are observed during the experiment in reflection and in transmission. Thus the PDH error signal is based on the expression for $P_{ref} = E_{ref}^* E_{ref}$, which in simplified terms yields:

$$P_{ref} = (\text{constant power terms in } \omega \text{ and } \Omega) + \epsilon(t)$$

In the usual case with a relatively low modulation frequency, the P_{ref} expression takes the form:

$$P_{ref} \approx (\text{constant term}) + P_0 \frac{d|F|^2}{d\omega} \Omega\beta \cos \Omega t + (\text{terms in } 2\Omega)$$

To obtain the signal in Ωt that samples the phase modulation, it is necessary to use a mixer of the output with a local oscillator at Ω, and using a low-pass filter to yield a near-DC signal.

The error signal is then just:

$$\epsilon(t) = P_0 \frac{d|F|^2}{d\omega}\Omega\beta \approx 2\sqrt{P_c P_s}\frac{d|F|^2}{d\omega}\Omega$$

as $\sqrt{P_c P_s} = \sqrt{J_0(\beta)^2 P_0 \cdot J_1(\beta)^2 P_0} \approx P_0 \cdot (\beta/2)$ using a Taylor approximation of $J_0(\beta)J_1(\beta)$ for low β

Depending on the modulation frequency Ω, after demodulation and low-pass filtering, ϵ(t) can take two different forms, both of them sharing the property of anti-symmetry around resonance values in frequency space:

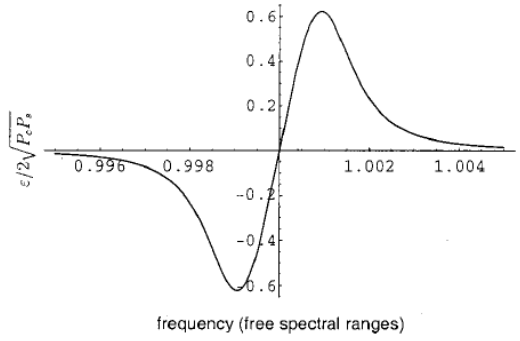

The Pound–Drever–Hall error signal, $\epsilon/2\sqrt{P_c P_s}$ vs $\omega/\Delta\nu_{\rm fsr}$, when the modulation frequency is low. The modulation frequency is about half a linewidth: about 10^{-3} of a free spectral range, with a cavity finesse of 500.

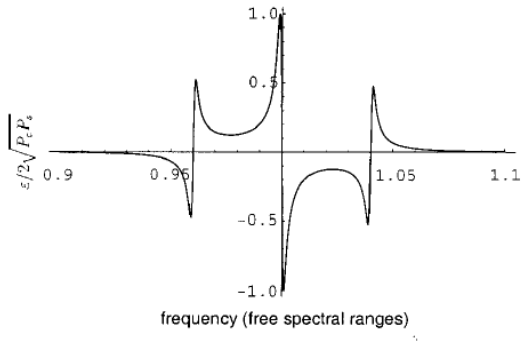

The Pound–Drever–Hall error signal, $\epsilon/2\sqrt{P_c P_s}$ vs $\omega/\Delta\nu_{\rm fsr}$, when the modulation frequency is high. Here, the modulation frequency is about 20 linewidths: roughly 4% of a free spectral range, with a cavity finesse of 500.

Fig. 2.3.1: Plots of the error signal (normalized to be dimensionless) for both low ($\frac{\Omega}{c/2L} = 10^{-3}$) and high ($\frac{\Omega}{c/2L} = 4 \cdot 10^{-2}$) modulation frequencies. P_c and P_s designate carrier and sideband powers respectively [12]

The important feature to these error signals is the (anti-)symmetry around resonance points; this allows to setup a suitable feedback control system and thus stabilize the frequency. The experimentally obtained signal had the characteristic symmetry (Fig. 2.3.2):

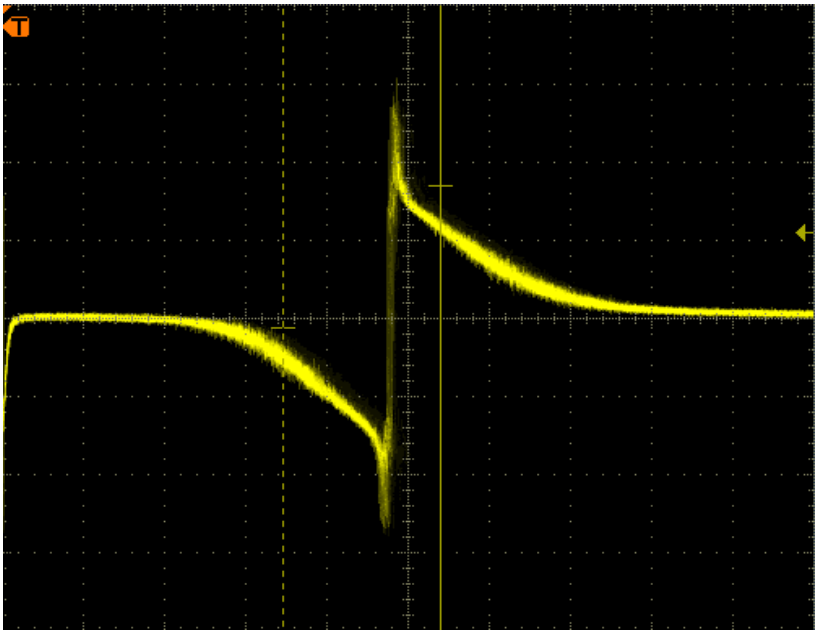

Fig. 2.3.2: Screenshot of the error signal obtained experimentally.

The setup used to establish this feedback control system attached to the laser path and cavity is illustrated below:

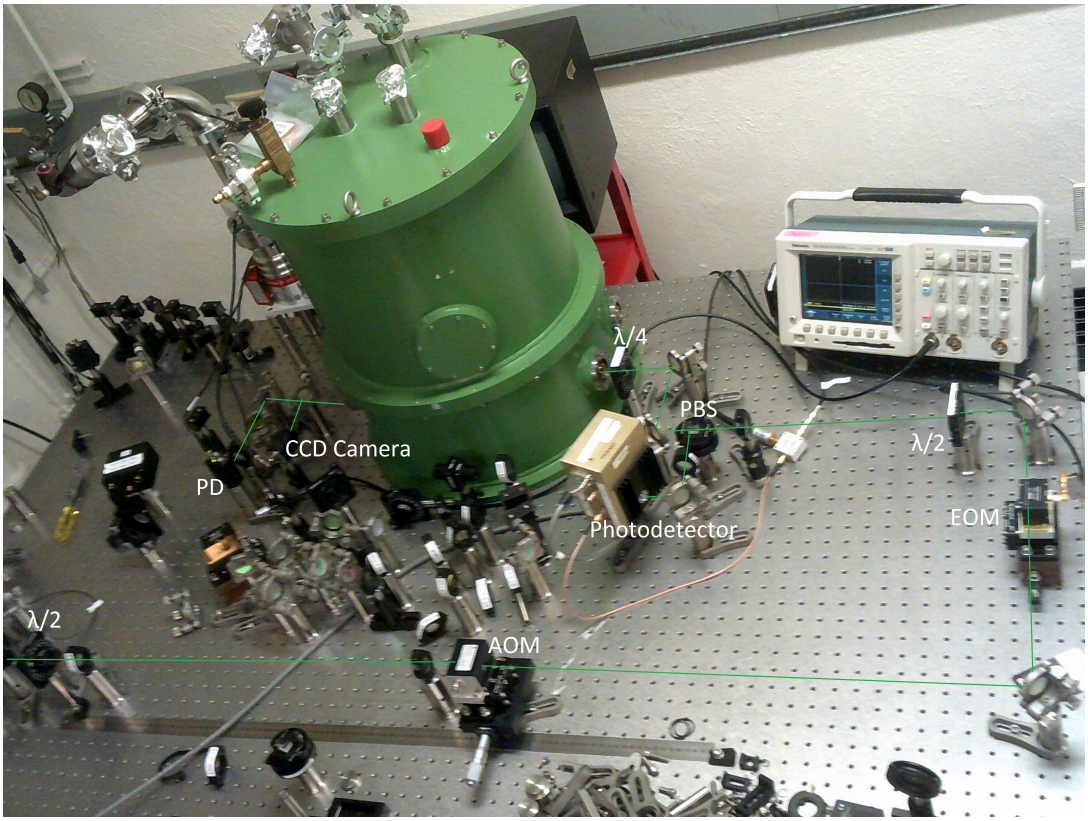

Fig. 2.3.3: Photo of the experimental setup

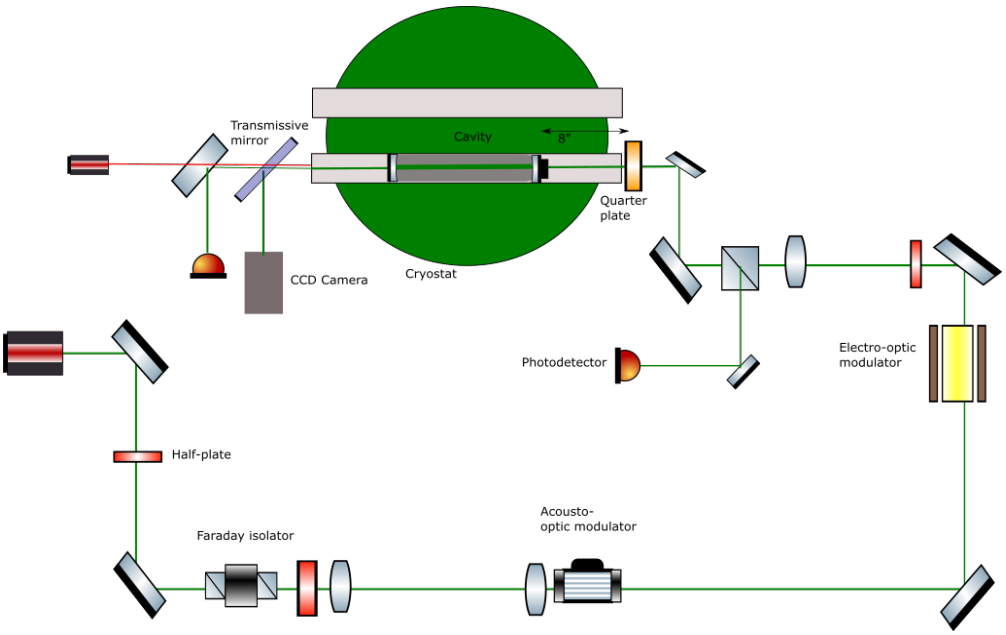

Fig. 2.3.4: Sketch of the components in the experimental setup from Fig. 2.3.3.

Description of some of the components in Fig. 2.3.4:

• **Half wave-plates and quarter wave-plates**: these plates serve to ensure correct incident polarization settings for components such as Faraday isolator (which is used to avoid back-reflection hitting the laser source) and polarizing beam-splitter (to pick off a reflected beam towards a photodetector in the perpendicular direction to the beam path)

• **Electro-optic modulator:** crucial element in the PDH technique. It introduces phase modulation in the incident beam, at a tunable Ω frequency.

• **Photodetectors:** they intercept incident laser beams as photovoltages.

• **CCD camera:** it intercepts the transmitted beam from behind the cavity

• **Servo (with proportional-integral controller):** Given the output error signal, it feeds back into the laser driver. *(not in the figure)*

2.4 Temperature modulation:

As mentioned in the beginning of Section 2, once the laser is locked to the cavity, it will be useful to test its response to thermal disturbances at room temperature and then desirably at 123 K, around the zero-crossing point for the CTE.

The method that will be used to cause these disturbances is called **temperature modulation**. It involves injecting a time-varying (preferably sinusoidal, at some frequency f_m)

amount of heat into the cavity, and observing the response of the cavity. An extra thermal "push" introduces thermo-elastic disturbances on its own, due to slight length imbalances around the resonance condition. This effect is marked at lower temperatures (ultimately near the root of the CTE), where the extra thermal injection sharply contrasts with the near-absence of intrinsic thermo-elastic jittering.

To cause such a temperature modulation, a secondary laser was introduced to the system. This laser is a modified laser pointer, with a time-varying input voltage (in contrast to the usual DC voltage from a battery). At this rudimentary level, the input voltage was chosen within the limits of the laser (given the nominal 3V battery marking), and thus had the form: $V(t) = V_0 + V_1 \sin(2\pi f_m t)$ with a $V_0 = 2.2$ V, and $V_1 = 0.7$ V. Having this functional form with a bias voltage translates into a transmitted bias in the heat input: the net amount of heat deposited onto the cavity mirror is positive, and is expected to fluctuate around that bias at f_m. The expected result from this heating technique should be a spectral response at that specific f_m incorporated into the behavior of the cavity while responding to the PDH feedback loop and the extra heating.

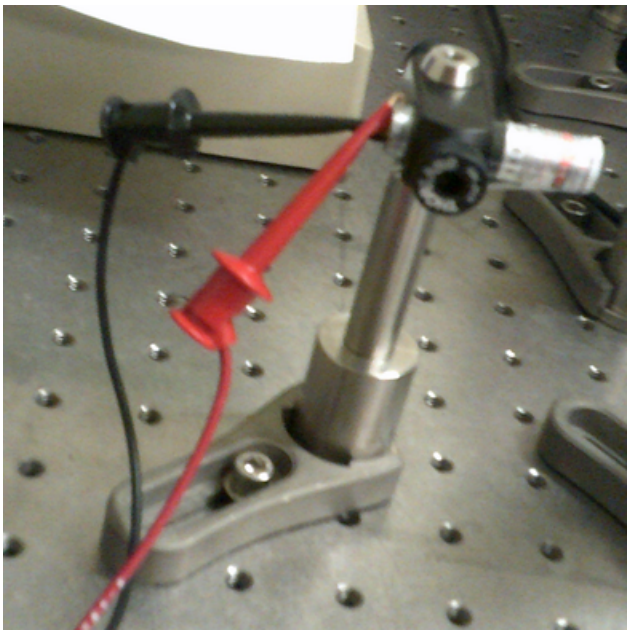

Fig. 2.4.1: Photo of the secondary laser, connected to a function generator

To detect the response of this temperature modulation (first at room temperature), two detection methods were devised:

• Detecting the modulation frequency as a peak in the feedback signal to the laser: this was inconclusive as the laser noise background is too high for a feeble peak from the heating laser to be resolved.

• A more indirect method: A beat note from the main laser and an additional laser from a reference cavity in the laboratory was obtained. Once that beat note was obtained, its frequency noise spectrum was extracted from the feedback signal to a function generator

that was phase-locked to the beat signal. The spectral readout of the thermal variations of this beat note were linked to the used modulation frequency f_m, as the spectral peak is high enough to pierce through the ambient noise ceiling (Fig. 2.4.2). This has been observed for varying values of f_m.

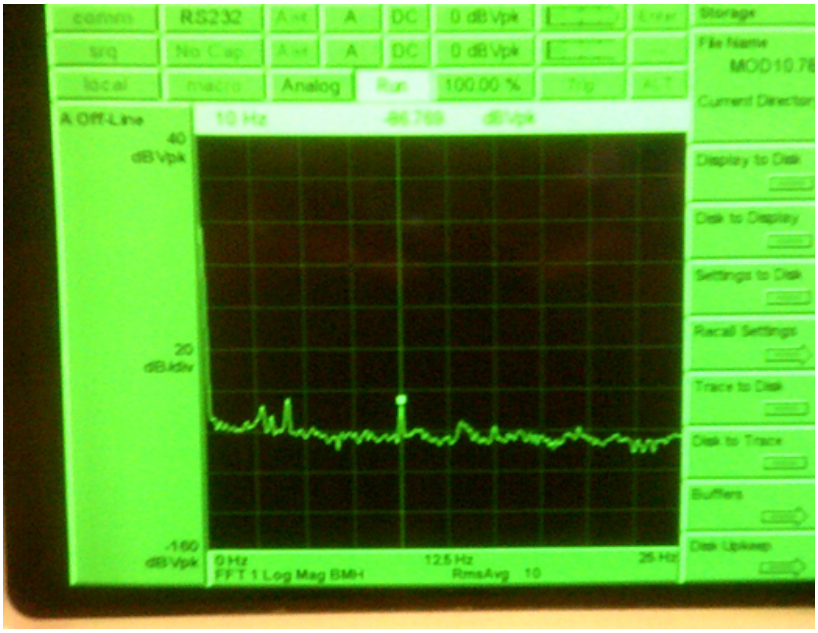

Fig. 2.4.2: Spectral readout of the temperature modulation peak using $f_m = 10$ Hz.

3 Conclusions and future steps

The first part of the project involved setting up a cavity and locking a laser to it using the Pound-Drever-Hall technique. This was obtained successfully, with T_{00} modes persisting on a time scale of hours, in contrast to the few seconds in the absence of frequency stabilization. The second part of the project involved the original investigation of the tentative temperature modulation system with the help of an auxiliary laser beam, driven sinusoidally. This has been tested at room temperature, and the response of the cavity observed for f_m values in the range of $1 - 10$ Hz.

Given that, an objective in the near future would be to try this modulation scheme at the target temperature region, near the CTE zero-crossing. At that point, work will have to be done in determining a temperature control system based on the zero-crossing property of the $\alpha(T)$ curve, in order not to stray far away in T space. But before that, a recommended fix to the system would be obtaining a better-performing auxiliary laser; the current one has severe power limitations, and came with an *ad hoc* wavelength setting (as do all optical range commercial laser pointers). Obtaining a high-intensity auxiliary laser would also provide a stronger spectral response in the cavity.

References

[1] B. P. Abbott *et al.*, "Observation of Gravitational Waves from a Binary Black Hole Merger", *Phys. Rev. Let.*, (2016)

[2] LIGO Optics (*https://www.ligo.caltech.edu/page/optics*)

[3] K. Arai, "Gravitational wave detection with laser interferometers", LIGO-G1601395-v1 (slides), (2016)

[4] L. Yu, "Internal thermal noise in the LIGO test masses: A direct approach", *Physical Review*, (1997)

[5] P. G. Murray *et al.*, "Ion-beam sputtered amorphous silicon films for cryogenic precision measurement systems", *Phys. Rev. D.*, (2015)

[6] R. Nawroft *et al.*, "High mechanical Q-factor measurements on silicon bulk samples", *Journal of Physics: Conference Series 122*, (2008)

[7] S. Rowan *et al.*, "Test mass materials for a new generation of gravitational wave detectors", *Proc. of SPIE Vol. 4856*, (2003)

[8] C. A. Swenson, "Recommended Values for the Thermal Expansivity of Silicon from 0K to 1000K", *J. Phys. Chem. Ref. Data, Vol. 12, No. 2*, (1983)

[9] D. Yeaton-Massey, "Cryogenic Silicon Optical Reference Cavities", *Thesis at California Institute of Technology*, (2016)

[10] H. Kogelnik and T. Li, "Laser Beams and Resonators", *Applied Optics (Vol. 5, No. 10)*, (1966)

[11] S. A. Self, "Focussing of spherical Gaussian beams", *Applied Optics (Vol. 22, No. 5)*, (1983)

[12] E. D. Black, "An introduction to Pound-Drever-Hall frequency stabilization", *American Association of Physics Teachers*, (2001)